The Effect of a CO_2 Laser Pulse Shape on the Accuracy of DIAL Measurements

AVISHAI BEN-DAVID

Science and Technology Corporation, Edgewood, Maryland

ALAN P. FORCE, FRANCIS M. D'AMICO, AND SILVIO L. EMERY

U.S. Army Chemical Research, Development, and Engineering Center, Aberdeen Proving Ground, Maryland

(Manuscript received 5 March 1991, in final form 16 December 1991)

ABSTRACT

The temporal pulse shape varies at different wavelengths, within the same wavelength, and between identical lasers. In differential absorption lidar (DIAL) measurements the variance introduced into the deduced average pathlength concentration from variation of laser pulse shape through the approximation of the normalized energy of the lidar return by sampling peak power values is small but can be significant for detecting low-level concentrations. The magnitude of this uncertainty is on the order of that caused by measurement errors on the order of a few percent.

1. Introduction

Carbon dioxide (CO_2) laser-based single-ended (receiver/transmitter collocated) lidar systems have been used to demonstrate the utility of differential absorption lidar (DIAL) in the 9–11-μm wavelength range for long-range remote sensing of trace molecular species in the atmosphere (Murray and van der Laan 1978; Killinger and Menyuk 1981; Menyuk et al. 1980; and Asai et al. 1979).

The single-scattering lidar equation is used to deduce the path-integrated concentration of the trace gas between the lidar and a target (topographic or a retroreflector) and is given by

$$P_r = P_t K \beta \frac{A}{R^2} \exp[-2(\sigma_m \rho_m + \alpha_a)R] \quad (1)$$

where P_r is the instantaneous received power of the backscattered lidar-transmitted power P_t after being backscattered from a target at a distance R (m) and a reflectance β (sr^{-1}). A typical temporal profile of the transmitted lidar pulse is given in Fig. 1. The received lidar power P_r is retarded by the time required for a round trip to a target at a distance R. Here A is the receiver telescope area, K the overall system constant, σ_m (m^2) the molecular absorption cross section of the specific molecular gas of interest, ρ_m (m^{-3}) the average concentration of the specific molecular gas of interest along R, and α_a (m^{-1}) in the background volume extinction coefficient of all other gases and aerosols in the atmosphere excluding the gas of interest.

In the DIAL technique the laser is tuned to two wavelengths. The first wavelength is chosen such that it will be absorbed heavily by the trace gas of interest. The second wavelength is chosen to be outside the absorption band of the gas and serves as a reference measurement to calibrate the reflectivity of the target.

The averaged pathlength concentration ρ_m can be computed from (1) when the laser is tuned to the maximum absorption of the specific gas (resonant wavelength), and to a wavelength outside the absorption maxima (nonresonant wavelength) and is given by

$$\rho_m = \frac{\ln\left(\frac{E_r/E_t}{E_r'/E_t'}\right)}{2(\sigma_m' - \sigma_m)R} + \frac{\ln(\beta'/\beta) + 2(\alpha_a - \alpha_a')R}{2(\sigma_m' - \sigma_m)R} \quad (2)$$

where the primed and unprimed parameters refer to values at nonresonant and resonant wavelengths, respectively, and E is the energy (i.e., the integral of the instantaneous power P) in the received or transmitted power.

For closely spaced on and off resonant wavelengths, the target reflectance β and the background volume extinction coefficient α are approximately constant with wavelength, and thus, ρ_m is given by the first term of (2). Error analysis of the average concentration uncertainty in (2) has been studied by many authors. Menyuk and Killinger (1983) studied the effect of atmospheric turbulence on fluctuations in the measured signal and the possible reduction of the turbulence effect by transmitting the two different wavelengths a few tens of microseconds apart in a dual-laser experi-

Corresponding author address: Dr. Avishai Ben-David, Science and Technology Corporation, 2719 Pulaski Highway, Unit 1, Edgewood, MD 21040.

ment. Cvijin et al. (1987) and Grant (1982) studied the effect of differential spectral reflectance on the DIAL technique. Modeling- and calibration-error considerations were addressed by Kavaya and Menzies (1985). In their paper they computed the error resulting from the assumption of a rectangular pulse shape on the backscattering from a diffused target (i.e., aerosols) and its effect on the DIAL technique.

In this paper we will examine the uncertainty in topographic DIAL measurements from variation of laser pulse shape introduced through the approximation of the normalized lidar return E_r/E_t by sampling peak-power values. The accuracy of approximating the normalized energy with peak-power values depends on the variation of the laser pulse shape during the measurements. Pulse shapes of CO_2 laser for different wavelengths were measured and its effect on DIAL computation for trace-gas detection is presented.

2. Pulse-energy normalization

The normalized lidar return can be measured in two ways. The first is to measure the transmitted and received energies by integrating the laser temporal pulse shapes and then to normalize on a pulse-to-pulse basis. The integration of the laser pulse can be done in hardware or in software (i.e., numerical integration of the digitized waveform). In this case the normalized return of N laser pulses is given by

$$\left\langle \frac{E_r}{E_t} \right\rangle = \frac{1}{N} \sum_{i=1}^{N} \frac{(E_r)_i}{(E_t)_i}. \tag{3}$$

A pulse-to-pulse normalization requires either a large mass storage system where the dual-wavelength digitized waveform pairs are stored and from which a normalized average will be computed, or a fast on-line computation in the data-acquisition system where a real-time normalization will be carried out. Often, for simplicity, the return and transmitted energies are summed separately and the sums are divided at the end of the measurements. The approximated ensemble average is given as

$$\frac{\langle E_r \rangle}{\langle E_t \rangle} = \frac{\frac{1}{N} \sum_{i=1}^{N} (E_r)_i}{\frac{1}{N} \sum_{i=1}^{N} (E_t)_i}. \tag{4}$$

The difference in results between (3) and (4) has been shown to be as large as 10% in SO_2 concentrations integrated over a plume at a distance of 900 m for laser energy fluctuations of 10% (Staehr et al. 1985), thus showing the effect of pulse-to-pulse energy fluctuation on the computed normalized lidar return signal. To reduce the effect of pulse-to-pulse energy fluctuation a pulse-to-pulse normalization [as seen in (3)] is implemented by measuring the peak of the transmitted and received signals. Thus, a complete waveform for every pulse is not necessary and only two data points for the return and transmitted pulses are sampled.

Let the ratio of a pulse energy E to its peak power S be C_r for the received power and C_t for the transmitted power (i.e., $C_r = E_r/S_r$, $C_t = E_t/S_t$). Using the peak power measurements, the average pathlength concentration ρ_m in (2) is given by

$$\rho_m = \frac{\ln\left(\frac{S_r/S_t}{S_r'/S_t'}\right)}{2(\sigma_m' - \sigma_m)R} + \frac{\ln\left(\frac{C_r/C_t}{C_r'/C_t'}\right)}{2(\sigma_m' - \sigma_m)R} + \frac{\ln(\beta'/\beta) + 2(\alpha_\alpha - \alpha_\alpha')R}{2(\sigma_m' - \sigma_m)R}. \tag{5}$$

The parameters C_r and C_t are a function of the convolution between the temporal pulse shape, the detector time-response function, and the amplifier time response. The parameters C_r and C_t will be noted as shape factors for the temporal pulse shapes. In a typical lidar system, such as the one to be described, a very sensitive [D^* (peak wavelength, 1 kHz) = 10^{10} cm $Hz^{1/2}$ W^{-1}] and slow (rise time = 0.3 μs) cooled liquid nitrogen mercury cadmium telluride (MCT) is used to measure the received power P_r, while a less sensitive [D^* (peak wavelength, 2 kHz) = 10^8 cm $Hz^{1/2}$ W^{-1}] and fast (rise time = tens of nanoseconds) room-temperature MCT is used to measure the transmitted power P_t. Therefore, the parameters C_r and C_t are not the same in most cases. The contribution of the pulse-shape variation [the second term in (5)] on the variance of the average pathlength concentration ρ_m is given by $(\text{var})_{\rho m}$ as follows:

$$(\text{var})_{\rho_m} = \frac{[(\text{var})_a/a^2] + [(\text{var})_b/b^2] - 2(\text{cov})_{a,b}\{[(\text{var})_a(\text{var})_b]^{1/2}/ab\}}{4(\sigma_m' - \sigma_m)^2 R^2} \tag{6}$$

where $a = C_r/C_t$, $b = C_r'/C_t'$, and $(\text{cov})_{a,b}$ denotes the covariance between a and b. The normalized variance of a and b is given by

$$\frac{(\text{var})_a}{a^2} = \frac{(\text{var})_{C_r}}{C_r^2} + \frac{(\text{var})C_t}{C_t^2} - 2(\text{cov})_{C_r C_t} \frac{[(\text{var})_{C_r}(\text{var})_{C_t}]^{1/2}}{C_r C_t}. \tag{6a}$$

The normalized variance of b is the same as (6a) when replacing the unprimed shape factors C_r and C_t with the primed shape factors C_r' and C_t'. The covariance between a and b, $(\text{cov})_{a,b}$, describes the correlation between the temporal shape of the on-resonant and the off-resonant laser pulses. The $(\text{cov})_{a,b}$ can be zero for two independent lasers used to transmit the two wavelengths or one laser that is tuned alternately

to the on-resonant and off-resonant wavelengths, and the pulses are uncorrelated. The $(\text{cov})_{a,b}$ will be ± 1 for a complete correlation of the on-resonant and off-resonant pulse shapes. The covariance between the received and transmitted power for the same laser pulse (wavelength) is one [i.e., $(\text{cov})_{C_r C_t} = (\text{cov})_{C_r' C_t'} = 1$ because C_r and C_t are a measure of the same laser pulse shape with different detectors].

The contribution of the pulse-shape variation to the variance of the averaged pathlength concentration will go to zero if the pulse shape remains constant. In this case peak-sensed DIAL measurements will be proportional to the integrated waveform (i.e., pulse-energy) measurements when (3) will be implemented for the averaging process. The proportionality constant will depend on the different time response of the detectors and the amplifiers used for the measurements but will not introduce random errors to ρ_m.

3. Experimental results and discussion

A block diagram of the dual CO_2 DIAL system is shown in Fig. 2. The two lasers used in this study were line-tunable Tachisto model 555G TEA CO_2 lasers. The lasers have been modified to increase the stability of the electrodes during operation. An intracavity iris was used to control the transverse modes. These lasers can transmit up to 2 J per pulse at a pulse repetition frequency (PRF) up to 20 Hz and a beam divergence of about 6 mrad. The PRF was limited to 5 Hz by the data acquisition system. In a DIAL experiment the two lasers are tuned to different wavelengths and separately triggered with a time delay of 5–50 μs to freeze the effect of the atmospheric turbulence (Menyuk and Killinger 1983).

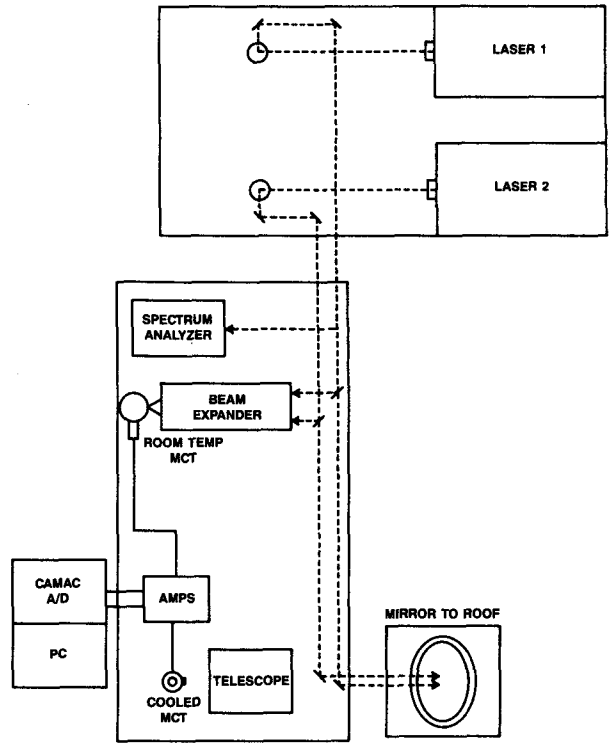

FIG. 2. A block diagram of the CO_2 DIAL laser system.

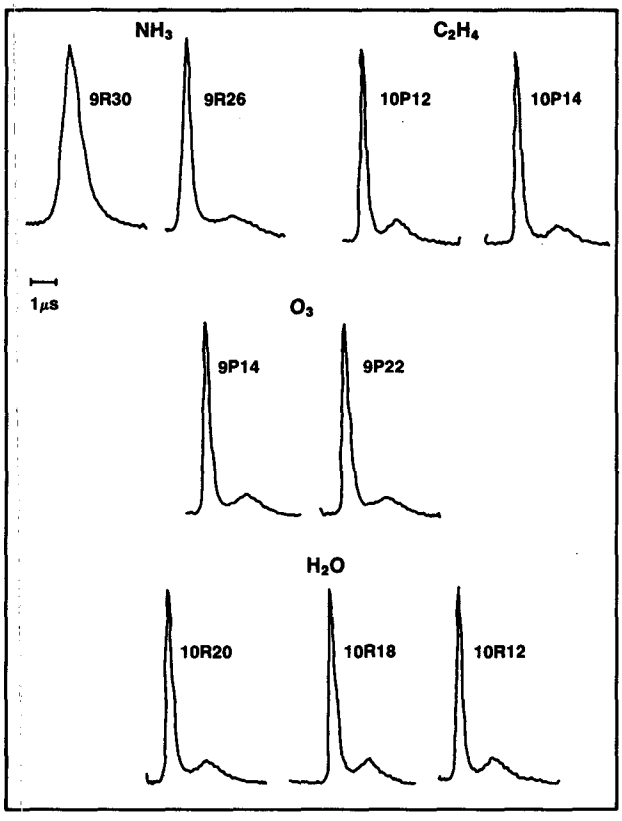

FIG. 1. Pulse shapes for nine CO_2 lines used in DIAL measurements for monitoring atmospheric trace gases NH_3, C_2H_4, O_3, and H_2O in the atmosphere.

The output pulses of the two lasers were directed in parallel beams to an observatory dome 20 m above the lidar. A 20-in. mirror mounted in the dome directs the beam toward a chosen target. The receiver field of view when using a 2-mm × 2-mm cooled liquid nitrogen MCT with a 4× germanium immersion lens and a f/3 Ritchey–Chretien 12-in. telescope was about 8 mrad.

For this experiment the doors of the dome were closed and were used as a target so that the pulse shape will not be affected by the atmosphere. The transmitted power was detected with a room-temperature MCT via a 10% beam splitter. The two split beams were recollimated via an off-axis, afocal Dall–Kirkham 6-in. telescope (e.g., a beam expander) into an integrating 5-in. sphere. The signals from the two detectors were amplified by 40-MHz bandwidth amplifiers and were sampled by a pair of 100-MHz waveform digitizers. The digitized signals were stored on a personal com-

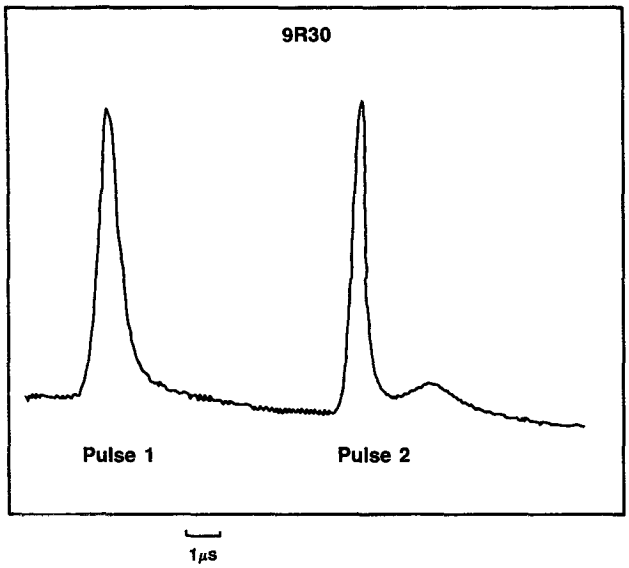

FIG. 3. A pulse shape of two consecutive laser pulses for the on-resonant CO_2 line used for NH_3 DIAL measurements.

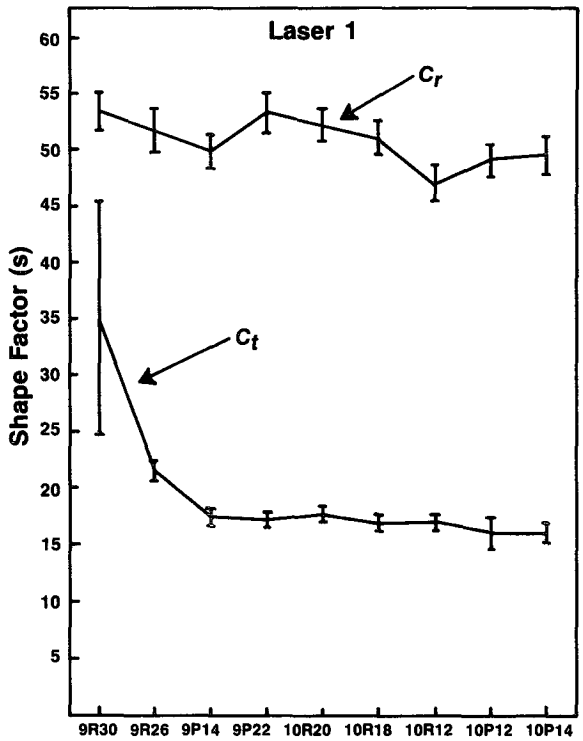

FIG. 4. Pulse-shape factors C_r and C_t as measured by two detectors (a room-temperature MCT and a cooled liquid nitrogen MCT) when the laser source is laser 1.

puter/AT where a numerical integration for the pulse energy and a peak value were computed for each pulse. Typically a set of at least 100 pulses was recorded at each wavelength with each detector. Neutral density filters were used to avoid saturation of the detectors. The 40-m round trip (260 ns) in the observatory dome was long enough for the RF noise produced by the laser at the time of energy discharge (i.e., laser firing) to decay significantly before measurements were recorded with the cooled liquid nitrogen MCT. The signal-to-noise ratio for a single pulse was about 50.

Figure 1 shows commonly used wavelengths for DIAL measurements of four gases: ammonia (NH_3), ethylene C_2H_4, ozone (O_3), and water vapor (H_2O). This figure shows the differences in the temporal pulse shape for the different wavelengths as was measured with a room-temperature MCT detector with a time constant of few tens of nanoseconds. An example of two consecutive pulses at the 9R30 laser line used for the ammonia DIAL experiment is given in Fig. 3. Figures 1 and 3 show the differences in the pulse shapes for CO_2 lines (wavelengths) and the temporal variation between pulses of any single wavelength. The list of wavelengths corresponding to the CO_2 laser lines is given in Table 1. The pulse shape measured by the cooled liquid nitrogen MCT is much wider than the pulse shape given in Fig. 1 as a result of the long time constant of the detector (0.3 μs). An analysis and description of the mechanism governing the pulse shape as a function of laser gas mix (i.e., the ratio between $He:CO_2:N_2$) is given by Zhao et al. (1988). Discussion of the change in pulse shape between "identical" lasers and laser during operation is beyond the scope of this study.

The ensemble average of at least 100 pulses was re-

TABLE 1. Laser lines, wavelengths, and absorption coefficient values for four common atmospheric gases (NH_3, C_2H_4, O_3, and H_2O).

Atmospheric gas	Laser line	Wavelength (μm)	Absorption coefficient (cm^{-1} atm^{-1})	Source
NH_3	9R30	9.219	56.1	Force et al. (1985)
	9R26	9.239	0.1	
C_2H_4	10P14	10.532	32.1	Killinger and Menyuk (1981)
	10P12	10.513	4.33	
O_3	9P14	9.504	13.0	Shumate et al. (1981)
	9P22	9.569	1.9	
H_2O	10R20	10.247	8.65×10^{-4}	Murray et al. (1976)
	10R18	10.260	0.935×10^{-4}	
	10R12	10.304	1.6×10^{-4}	

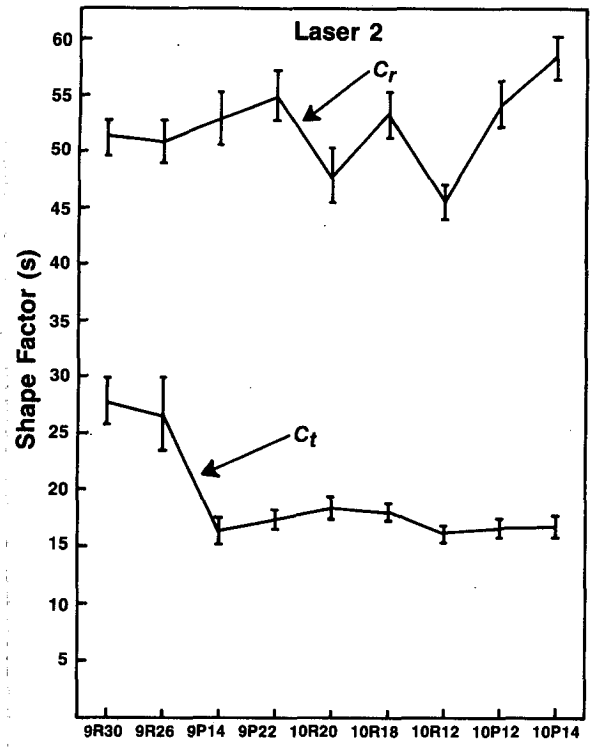

FIG. 5. The same as Fig. 4 but when the laser source is laser 2.

corded for each wavelength. For each recorded pulse the energy and the peak value were computed and the ratio (i.e., the shape factor) was calculated. The average value and the standard deviation of the shape factor are presented in Figs. 4 and 5. The figures show the shape factors C_r and C_t for the two detectors when the two Tachisto lasers were used. The shape factors were calculated at the nine wavelengths that are commonly used for detecting the four atmospheric gases NH_3, C_2H_4, O_3, and H_2O. These figures show that the two lasers exhibit different pulse-shape characteristics for these wavelengths. The difference between the average value of the shape factor across the wavelength (i.e., between on-resonant and off-resonant wavelengths) will cause a systematic error in the computed average pathlength concentration [see (5)]. This systematic error [the second term in (5)] can be corrected. The random fluctuation of the shape factor, even for a large ensemble average, cannot, however, be corrected and will contribute to the variance of the computed average path concentration ρ_m.

The standard deviation of the average pathlength concentration (over a 1-km pathlength), as a result of the pulse-shape variation for the four atmospheric gases, was calculated through (6) and is shown in Table 2. The absorption coefficients for the on-resonant and off-resonant wavelengths are shown in Table 1. Table 2 shows the uncertainty (ppb km) in the average path concentration ρ_m, under different combinations of laser 1 and laser 2 that were used to transmit the on-resonant and off-resonant wavelengths. Because the two lasers are not identical as far as pulse shape is concerned, the uncertainty in ρ_m depends on the choice of lasers for the on-resonant and off-resonant wavelengths. For example, even though a dual-laser DIAL experiment (Killinger and Menyuk 1981) will reduce the received signal fluctuation, this improvement can be decreased greatly because of pulse-shape variation of the two lasers. A single-laser DIAL experiment to measure NH_3 with laser 2 will give better results than a dual-laser experiment with laser 1 set on line 9R30 (on resonance) and laser 2 set on line 9R26 (off resonance). For these CO_2 laser lines, a dual-laser experiment with laser 2 on 9R30 and laser 1 on 9R26 will give the smallest uncertainty in ρ_m. The last column in Table 2 shows the minimum detectable average pathlength concentration when the only uncertainty is in the received

TABLE 2. Average pathlength concentration for four trace gases (NH_3, C_2H_4, O_3, and H_2O).

Atmospheric gas	Covariance coefficients between on- and off-resonant pulses	Single-laser DIAL: Laser 1 on resonant, Laser 1 off resonant uncertainty	Single-laser DIAL: Laser 2 on resonant, Laser 2 off resonant (ppb km)	Dual-laser DIAL: Laser 1 on resonant, Laser 2 off resonant uncertainty	Dual-laser DIAL: Laser 1 off resonant, Laser 2 on resonant (ppb km)	Minimum detectable concentration for 2% in measurement (ppb km)
NH_3	0	23.3	8.2	24.4	3.2	1.8
	1	22.9	4.4	15.7	2.9	
C_2H_4	0	11.3	2.4	1.9	11.1	3.6
	1	9.5	1.4	0.8	8.9	
O_3	0	5.2	11.3	4.7	11.6	9.0
	1	2.3	11.1	4.5	9.0	
H_2O ($10R_{20}$, $10R_{18}$)	0	6.6×10^5	1.8×10^5	1.2×10^5	6.7×10^5	1.3×10^5
	1	5.3×10^5	1.6×10^5	1.1×10^5	4.7×10^5	
H_2O ($10R_{12}$, $10R_{18}$)	0	9.4×10^6	2.2×10^6	5.6×10^6	7.8×10^6	1.5×10^6
	1	1.9×10^6	2.0×10^6	5.5×10^6	5.4×10^6	

power that is equal to the detector-noise equivalent power. The minimum detectable concentration is given by Killinger and Menyuk (1981) as:

$$(\rho_m)_{\min} = \frac{\Delta P/P}{2(\sigma_m' - \sigma_m)R} \tag{7}$$

where $\Delta p/p$ is the relative measurement error.

4. Conclusions

The uncertainty in topographic DIAL measurements from variation of laser pulse shape introduced through the approximation of the normalized lidar return E_r/E_t by sampling peak power values was presented. The accuracy of approximating the normalized energy with peak-power values depends on the variation of the laser pulse shape during the measurements. The uncertainty in the deduced average pathlength concentration is not large but can be significant when low-level concentration is to be detected. The uncertainty introduced by the pulse-shape variation is on the same order of magnitude as the minimum detectable concentration, as determined by a measurement error of a few percent. The pulse-shape variation can vary from wavelength to wavelength and can be different even for identical lasers. Therefore, an optimal combination of lasers for the on-resonant and off-resonant wavelengths can improve the sensitivity of the DIAL system. This selection can be done by a prior check of the pulse shape variation for each laser used and for the specific required CO_2 lines.

Acknowledgements. The discussions with Steven Gotoff of the U.S. Army Chemical Research, Development, and Engineering Center (CRDEC) are greatly appreciated. The authors wish to thank Felix Reyes of CRDEC for his administrative support.

REFERENCES

Asai, K., T. Itabe, and T. Igarashi, 1979: Range resolved measurements of atmospheric ozone using differential-absorption CO_2 laser radar. *Appl. Phys. Lett.*, **35,** 60–62.

Cvijin, P. V., D. Ignjatijevic, I. Mendas, M. Sreckovic, L. Pantani, and I. Pippi, 1987: Reflectance spectra of terrestrial surface material at CO_2 laser wavelengths: Effect on DIAL and geological remote sensing. *Appl. Opt.*, **26,** 4323–4329.

Force, A. P., D. K. Killinger, W. E. DeFeo, and N. Menyuk, 1985: Laser remote sensing of atmospheric ammonia using a CO_2 lidar system. *Appl. Opt.*, **24,** 2837–2841.

Grant, W. B., 1982: Effect of differential spectral reflectance DIAL measurements using topographic targets. *Appl. Opt.*, **21,** 2390–2394.

Kavaya, M., and R. T. Menzies, 1985: Lidar aerosol backscatter measurements: Systematic, modeling, and calibration error considerations. *Appl. Opt.*, **24,** 3444–3453.

Killinger, D. K., and N. Menyuk, 1981: Remote probing of the atmosphere using a CO_2 DIAL system. *IEEE J. Quantum Electron.*, **QE-17,** 1917–1929.

Menyuk, N., and D. K. Killinger, 1983: Assessment of relative error sources in the IR DIAL measurement accuracy. *Appl. Opt.*, **22,** 2690–2698.

——, ——, and W. E. DeFeo, 1980: Remote sensing of NO using a differential absorption lidar. *Appl. Opt.*, **19,** 3282–3286.

Murray, E. R., and J. E. van der Laan, 1978: Remote measurement of ethylene using a CO_2 differential-absorption lidar. *Appl. Opt.*, **17,** 814–817.

——, R. D. Hake, Jr., J. E. van der Laan, and J. G. Hawley, 1976: Atmospheric water vapor measurements with an infrared 10 μm differential absorption lidar system. *Appl. Phys. Lett.*, **28,** 542–543.

Shumate, M. S., R. T. Menzies, W. B. Grant, and D. S. McDougal, 1981: Laser absorption spectrometer: Remote measurement of tropospheric ozone. *Appl. Opt.*, **20,** 545–552.

Staehr, W., W. Lahmann, and C. Weitkamp, 1985: Range-resolved differential absorption lidar optimization of range and sensitivity. *Appl. Opt.*, **24,** 1950–1956.

Zhao, Y., T. K. Lea, and R. M. Schotland, 1988: Correction function for the lidar equation and some techniques for incoherent CO_2 lidar data reduction. *Appl. Opt.*, **27,** 2730–2740.